Analysis of an Axial Permanent Magnetic Bearing for 1MW Horizontal Axis Wind

Article · April 2022

DOI: 10.37934/arfmts.94.1.172187

9 authors, including:

Kriswanto Kriswanto
Universitas Negeri Semarang
19 PUBLICATIONS **23** CITATIONS
SEE PROFILE

Dony Hidayat Al-Janan
Universitas Negeri Semarang
16 PUBLICATIONS **51** CITATIONS
SEE PROFILE

Ahmad Roziqin Arrozi
Universitas Negeri Semarang
6 PUBLICATIONS **6** CITATIONS
SEE PROFILE

Samsudin Anis
Universitas Negeri Semarang
53 PUBLICATIONS **905** CITATIONS
SEE PROFILE

SEMARAK ILMU PUBLISHING

Journal of Advanced Research in Fluid Mechanics and Thermal Sciences

Journal homepage:
https://semarakilmu.com.my/journals/index.php/fluid_mechanics_thermal_sciences/index
ISSN: 2289-7879

Analysis of an Axial Permanent Magnetic Bearing for 1MW Horizontal Axis Wind Turbine

Kriswanto[1,*], Rizqi Fitri Naryanto[1], Renaldy Prasdiansyah[1], Dony Hidayat Al-Janan[1], Widya Aryadi[1], Ahmad Roziqin[1], Samsudin Anis[1], Wirawan Sumbodo[1], Jamari[2]

[1] Department of Mechanical Engineering, Universitas Negeri Semarang, Gd E9 Kampus Sekaran Gunungpati, Semarang, Indonesia
[2] Department of Mechanical Engineering, University of Diponegoro, Jl. Prof. Sudharto Kampus UNDIP Tembalang, Semarang 50275, Indonesia

ARTICLE INFO

Article history:
Received 12 November 2021
Received in revised form 10 March 2022
Accepted 13 March 2022
Available online 11 April 2022

Keywords:
Bearing; permanent magnetic bearing; horizontal axis wind turbine; axial force

ABSTRACT

One way to reduce maintenance costs while improving wind turbine efficiency is to replace mechanical bearings with permanent magnetic bearings. The permanent magnetic bearing is a free contact bearing in which the rotor is elevated from the stator by the magnet's repelling force. The purpose of this study is to analyze the variation of permanent magnet width and the gap distance between the rotor-stator magnets that can produce the magnetic axial force opposing the thrust force of 1MW horizontal axis wind turbines (HAWT). The method used in this study is a magnetic force simulation using finite element method by varying the magnet thickness, width of the gap, and displacement between the rotor-stator of the PMB model. The PMB model consists of rotor and stator magnets arranged in 3 layers with Nd2Fe14B type material with a magnetic flux density of 1.45 T. Variations in thickness of the rotor and stator magnets are 0.1; 0.15, respectively; 0.2 (m), while variations in the width of the magnetic gap are 4, 5, 6 (mm). The results of the study found that the displacement that produces an axial magnetic force that can support a thrust force of 199.5kN is the lowest in the PMB model with a magnetic thickness of 0.15m with a magnetic gap of 4mm, while the highest is at a magnetic thickness of 0.1m with a magnet gap of 6mm. The greater the thickness of the PMB axial magnet design, the greater the displacement that provides zero axial magnetic forces. Further, the maximum of the magnetic axial force is rise on with increasing magnet thickness.

1. Introduction

One of the most critical components of wind turbines is the bearing. Furthermore, the wind industry has recognized main bearing failures as a major concern in terms of raising wind turbine reliability and availability, according to the European Academy of Wind Energy (EAWE) [1]. It is due to the high maintenance costs and long periods of downtime related to main bearing failures. Large-scale power plants currently apply mechanical bearings for onshore and offshore wind turbines. Nevertheless, the use of it has a limited-service life as well as capability [2]. So, the effort to improve

** Corresponding author.*
Email address: kriswanto@mail.unnes.ac.id

https://doi.org/10.37934/arfmts.94.1.172187

the efficiency and reliability of wind turbines is to minimize friction using magnetic bearings [3]. The magnetic bearing is a bearing that utilizes refuse forces to support a rotor without physical contact [4].

Magnetic bearings have the benefit of being able to adapt to changing operating conditions and the environment. Within certain limits, the adjustment of magnetic bearing caused vibration was independent of the rotor position. Moreover, magnetic bearings can maintain rotor equilibrium positions at various loads. The rotor can rotate on its main axis and does not cause vibration on the foundation. Due to the levitation force of magnets, the vibration was significantly reduced [5]. The study of the magnetic bearing on the flywheel has the same polarity as the rotor, generating repulsive forces that keep the flywheel magnetically levitating and thereby reducing friction losses inside [6]. Nevertheless, permanent magnetic bearings (PMB) have several problems, including stability problems. Otherwise, given the long lifetime of its use then PMB is an effective solution to overcome the bearing problems [7]. The study of PMB in wind turbine prototypes to substitute mechanical bearings can enhance rotational speed and torque, therefore enhancing Horizontal Axis Wind Turbine (HAWT) performance [8]. Comparative study of axial force results of PMB between analytical approach and finite element method shows good agreement between the two [9].

The permanent magnetic bearing has been applied for rotating shafts that are used to replace conventional bearings which have high maintenance costs and friction [11]. Therefore, maintenance costs of wind turbines can be minimized by the use of permanent magnetic bearings. It is aligned with the statement that passive magnetic bearing is one of the most economical and effective methods to lift the two surfaces in relative motion that do not require active control and additional energy [12].

The study of modeling of the axial permanent magnetic bearing that comparing the theoretical simulation of the Monte Carlo method and the finite element method found that errors approximate zero and are consistent. Moreover, the experimental results are consistent with the simulation analysis [13]. The previous study [3-8] [10-12] shows the permanent magnetic bearings reduce friction, minimizes maintenance costs, can replace mechanical bearings. While none of the above literature has developed or studied the axial force of a PMB for a 1MW HAWT. The main shaft bearing of the HAWT must support both radial and axial loads (thrust forces). Furthermore, the HAWT thrust force is affected by the cut in and cut out of wind speed. The higher the wind speed, the higher the axial load on the main shaft bearing HAWT. Therefore, this paper presents to analyzes the axial magnetic force of the several thicknesses and air gaps of the permanent magnetic bearing models as the main bearing of the 1MW HAWT. Magnetic force and displacement are analyzed to find the shortest gap that can sustain the highest thrust force (at the cut out of wind speed). The main bearing locates near the gearbox, as shown in Figure 1 and indicated by number 2.

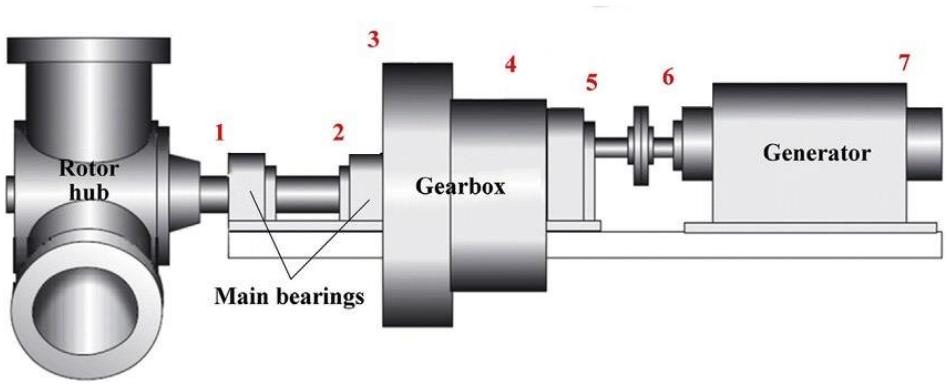

Fig. 1. Main shaft bearings [10]

2. Methodology

The main shaft of the HAWT model, made of 34CrNiMo6 steel, complies with wind turbine certification standards [14]. Furthermore, it was analyzed by finite element method and confirmed by Mohr II theory calculations to get the deflection value due to radial load. The defection will be used as the minimum air gap to prevent collisions between the rotor magnets and the stator magnets. The material properties of 34CrNiMo6 steel used in the finite element method are the density of 7800 (kg/m^3), elasticity modulus by 210 GPa, and Poisson's ratio of 0.3 [15]. The main shaft must be safe during operation to prevent damage that causes unexpected economic losses [16]. Furthermore, the 34CrNiMo6 steel has good toughness properties also the shock resistance of the material is good enough in the operating environment temperature [17]. In addition to being applied to wind turbine shafts, 34CrNiMo6 is high-strength structural steel frequently used in large-sized shaft components with complex geometry, such as aircraft propeller shafts and automobile connecting rods [18-19]. The specifications for the horizontal axis wind turbine show in Table 1.

Table 1
HAWT model specifications

Part name	Specification	Value
Rotor Blade	Number of blades	3
	Diameter (m)	54.4
	power coefficient, C_P	0.4877
	Tip Speed Ratio, TSR	2.82
	Rotor Load (N)	164150
Main shaft	Density, ρ (kg/m^3)	7800
	Diameter (m)	1.25
	Massa, *m* (Kg)	404.3
	Length, *l* (m)	4.5
	Material	34CrNiMo6
Bearing	Diameter Bore (m)	1.25
	Outer diameter (m)	2.2
	Material	$Nd_2Fe_{14}B$
	Remanent flux density, B_r (T)	1.45
Control	Cut in speed (m/s)	3.5
	Cut out speed (m/s)	15

The maximum deflection is the distance of the shaft to prevent the possibility of friction between the stator magnet and the rotor magnet. This calculation uses two methods, namely the finite element analysis method and Mohr's Theory calculation. Many uses of FEM in the structural field are to analyze stresses and displacements [20-24]. The bending moment diagram on the HAWT main shaft shows in Figure 2.

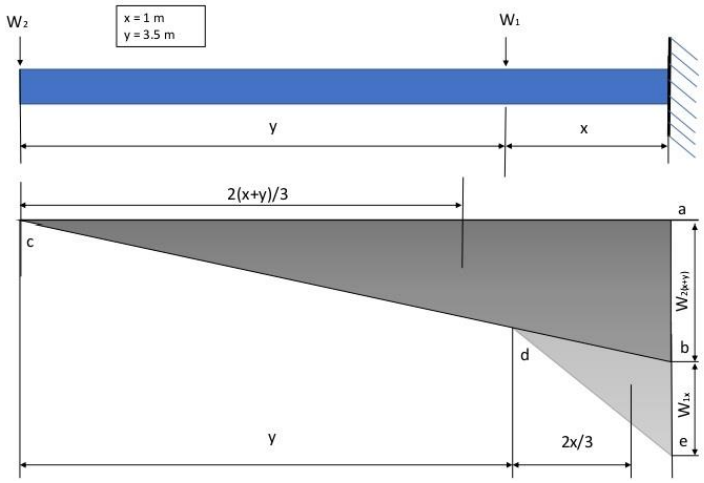

Fig. 2. Bending moment diagram of HAWT main shaft

which *x* (m) is the distance from the base of the shaft to the center of the magnetic load, y is the distance from the center of gravity to the end shaft (m), W_1 is the rotor magnet load (N), and W_2 is the total load from the connector hub load and the rotor load (N). Hereafter, the Eq. (1) and Eq. (2) for the deflection calculations.

$$I_P = \pi\, 4\, (r_{c2}{}^4 - r_{c1}{}^4) \tag{1}$$

$$\delta = \frac{1}{EI} \int_X^Y \mathrm{M}\, x\, \mathrm{d}x \tag{2}$$

where I_P is the polar inertia of the shaft, r_{c1} is the inner radius of the shaft cylinder, r_{c2} is the outer radius of the shaft cylinder, *E* modulus of elasticity of 34CrNiMo6, *M* is an area of the bending moment diagram, *x* is the distance of the load to the base of the shaft, and δ is the maximum deflection of the shaft. The data for each variable is present in Table 2.

Table 2
Properties on HAWT main shaft

x [m]	*y*[m]	W_1 [N]	W_2 [N]	r_{c1} [m]	r_{c2} [m]	*E* [GPa]
1	3.5	17,283	164,150	0.225	0.625	210

The location of the axial PMB on the HAWT main shaft is shown in Figure 3, wherein the position is closer to the gearbox. The free-body diagram of the force and moment on the main shaft see in Figure 4. The thrust force received by the rotor from the wind calculate using Eq. (4).

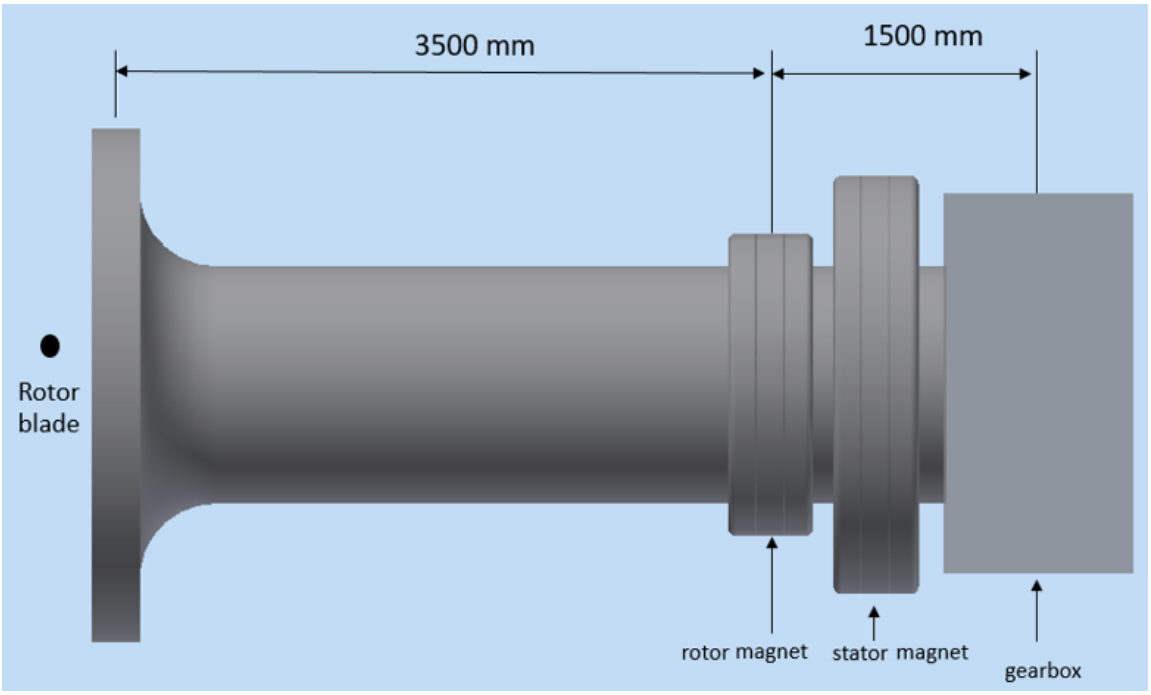

Fig. 3. Location of axial PMB on the HAWT main shaft

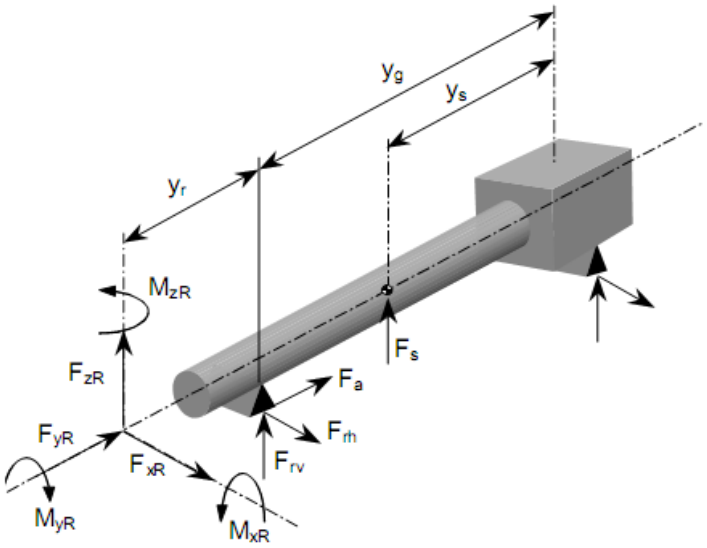

Fig. 4. Forces and moments on the HAWT main shaft [25]

$$A = \pi\, r2 \tag{3}$$

$$F_{yR} = \frac{1}{2}\,\rho\, A\,(v_1^2 - v_2^2) \tag{4}$$

The magnetic force simulation in this study uses the finite element method assisted of COMSOL by integrating vector Eq. (5). COMSOL software is a powerful modeling and simulation tool for engineering and industrial applications combining several physics connections [26]. The axial force of the PMB model was simulation by displacement distance between the rotor magnet against the stator.

$$f = n.T = -\frac{1}{2}n(H.B) + (n.H)B^T \tag{5}$$

where *f* is the magnetic force (n), *n* is the external normal vector, *T* is the tensor stress Maxwell, *H* is the magnetic field/ coercivity, *B* is the magnetic flux density (T).

The magnetic model uses the relationship between the density of the magnetic lines force and the magnetic field, which is expressed by Eq. (6).

$$B = \mu_r \mu_0 H \tag{6}$$

where μ_r is the relative permeability and μ_0 is the absolute magnetic permeability.

Magnetic field using Ampere's law model, with the stationary magnetic field Eq. (7).

$$B = \bar{V} A' \tag{7}$$

$$\mu_0{}^{-1} \mu_r{}^{-1} \overline{V} A' = J \tag{8}$$

where $\bar{V}$ is the vector operators, A' is the Magnetic potential vector, and J is the magnetization residual or magnetism induction density. Boundary conditions using the Eq. (9).

$$n_1 A' = 0 \tag{9}$$

The magnetic field was the model using a magnetic field interface model. Ampere's law used to include magnetic field physics into all free air domains. The infinite element domain uses to simulate the large region of free space surrounding the magnets. The material for all free domains is air. The free triangular mesh generated in the simulation is both the computational domain and the magnets. In this study, the magnet material made from $Nd_2Fe_{14}B$, which the magnet is composed of a mixture of neodymium (Nd), iron powder (Fe), and boron powders (B) using the high compression molding method [27]. The $Nd_2Fe_{14}B$ is a kind of hard magnet with excellent magnetic characteristics, possesses the highest values of maximum energy product (BH) max and coercivity [28-30]. In addition, $Nd_2Fe_{14}B$ is the strongest permanent magnet because maximum energy reaches more than 400kJ/m^3 [31-33]. Figure 5 show the HAWT main shaft design, all dimensional units of mm. The diameter of the HAWT main shaft is a limitation in determining the inner diameter of the PMB rotor magnet.

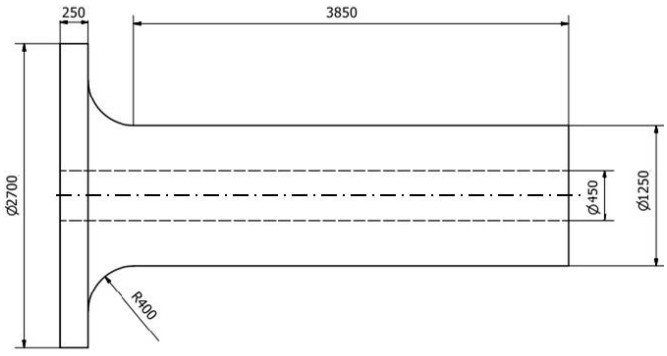

Fig. 5. HAWT main shaft design

As illustrated in Figure 6, the PMB axial configuration design includes three magnets on the rotor magnet *B* and the stator magnet *A*, which has a magnetic force density direction like in Figure. The rotor magnet is an inner magnet with an outer diameter smaller than the stator magnet's inner diameter, resulting in a gap. Placement of the rotor magnet against the stator, *LZ0* must be in a

condition where there is no axial magnetic force interaction between the two (F_z=0N). This setting is a condition when the wind turbine rotor does not receive thrust force from the wind. Meanwhile, the maximum thrust force or at the cut-out wind speed must restrain by the PMB thrust force with the smallest possible displacement distance (ΔZ).

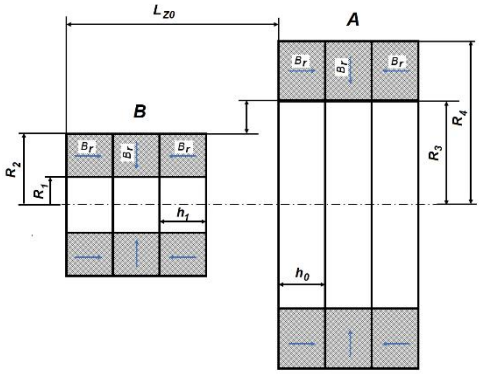

Fig. 6. Design of axial PMB configuration

The design specifications of the axial PMB model are presented in Table 3, wherein the model uses a configuration of concentric ring permanent magnets which have different dimensions and have opposite directions of magnetic force density (*Br*). Furthermore, the axial PMB in the present study functions as the axial main shaft bearing of HAWT.

Table 3
PMB model specifications

	Outer magnet, A	Inner magnet, B
Inner Radius (m)	R_3 = 0.805; 0.806; 0.8067	R_1 = 0.625
Outer Radius (m)	R_4 = 1.1	R_2 = 0.8
Thickness (m)	h_0 = 0.1; 0.15; 0.2	h_1 = 0.1; 0.15; 0.2
Magnetic Flux Density, *Br* (T)	1.45	1.45

3. Results

3.1 Thrust Force on The HAWT Main Shaft

The Thrust force (F_{yR}) of the HAWT main shaft is calculated by Eq. (3), which A of 2323.098 m^2 and ρ is the air density assumed is 1.293 kg/m^3. The thrust force results on the HAWT main shaft are shown in Figure 7.

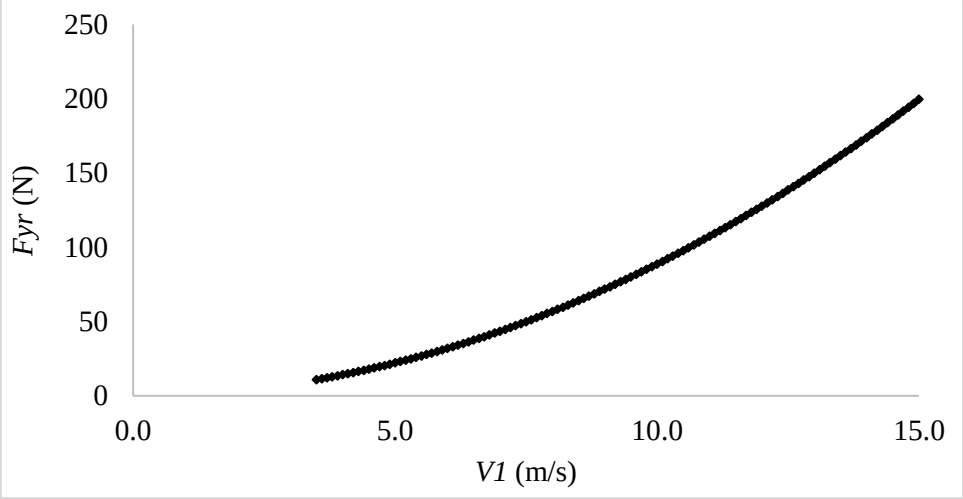

Fig. 7. Graph of the thrust force on the HAWT main shaft vs windspeed

The minimum thrust force is 10862.22 N generated at a wind speed of 3.5 m/s at the cut-in of HAWT, while the maximum is 199.5kN generated at a wind speed of 15 m/s, namely at a HAWT cut-out. The higher the wind speed, the higher the thrust force. According to Figure 7, the HAWT main shaft bearing must sustain an thrust force of 199.5 kN.

3.2 Maximum Deflection on The Main Shaft Of HAWT

The maximum deflection is analyzed to determine the minimum gap between the rotor magnets and the stator not to touch later. The results obtained from the finite element method (FEM) use COMSOL will then compare with mathematical of the Mohr II theoretical equation. The results of the maximum deflection analysis show in Figure 8.

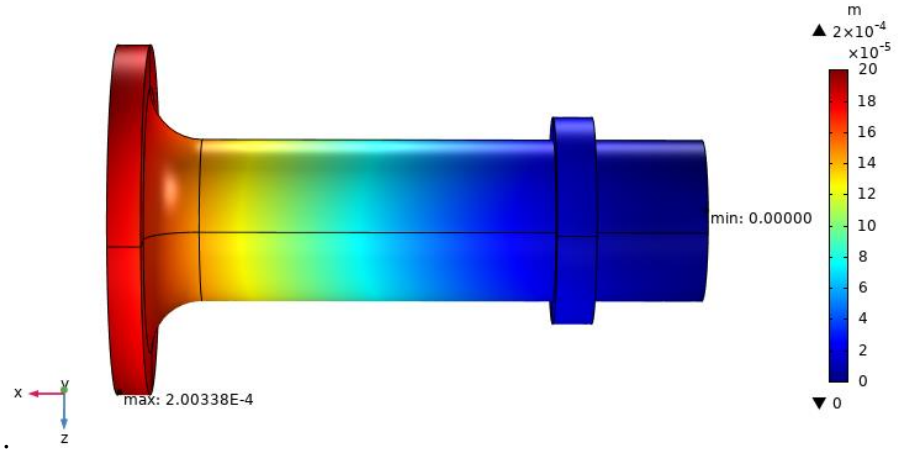

Fig. 8. Maximum deflection of HAWT main shaft use FEM

The maximum deflection of the modeling approximates analytic calculations using Mohr II theory (see Table 4). Moreover, the discrepancy between the two methods above has 0.015 %, which indicates that the FEM agrees with the analytic.

Table 4
Model Validation with Mohr II theory

	FEM	Analytic	Variation (%)
Maximum Deflection (mm)	0.20033	0.20036	0.015

3.3 PMB Model Validation

Figure 9 is a plot of axial force versus displacement generated from the modeling, where the axial force *Fz* is 126.12 N, is the rotor magnet experiences an of the stator as far as 6mm towards the positive axial direction *dZ*. This also applies to the displacement that leads to negative axial where at *dZ* at a distance of -6mm an axial force *Fz* equal to -126.12 N is produced.

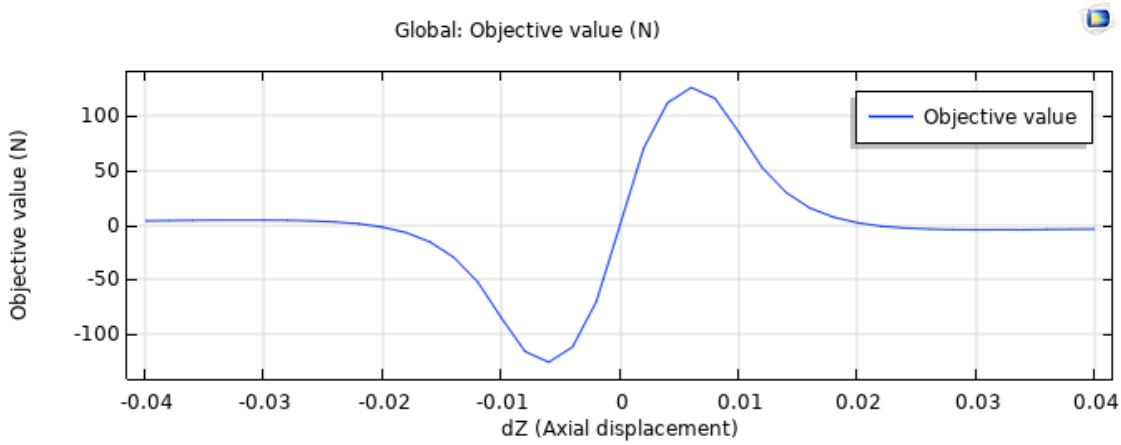

Fig. 9. Plot of the magnetic axial force of the modelling

The maximal axial force obtained through modeling is 126.12N, whereas the Bekinal mathematical model yields 126.59N (see Table 5). The discrepancy between the results of the two methods is 0.37%, which indicates that the modeling method is declared valid.

Table 5
Validation of the axial force with Bekinal model

	Modeling	Bekinal model [34]	Variation (%)
Axial Force (N)	126.12	126.59	0.37

3.4 Axial Force Modeling Of 0.1 M Magnet Thickness of the PMB

The axial PMB design is depicted in Figure 6, then the parameters provided in Table 1 have values of h_0-h_1 indicate a magnet thickness of 0.1 m. The variation in this configuration lies in the width of the magnetic gap with R_3 values are 0.805, 0.806, 0.807 (m), so that the magnetic gap *c* becomes 4 mm, 5 mm, and 6 mm. The maximum magnetic flux density of 1.45T (see Figure 10(a)) at 0.1 m thickness variation and 4mm gap as shown in the red area concentrated in the center of the magnet both on the rotor and stator. Figure 10(b) depicts the axial force towards displacement with *dZ* – 0.38 m to 0.38 m.

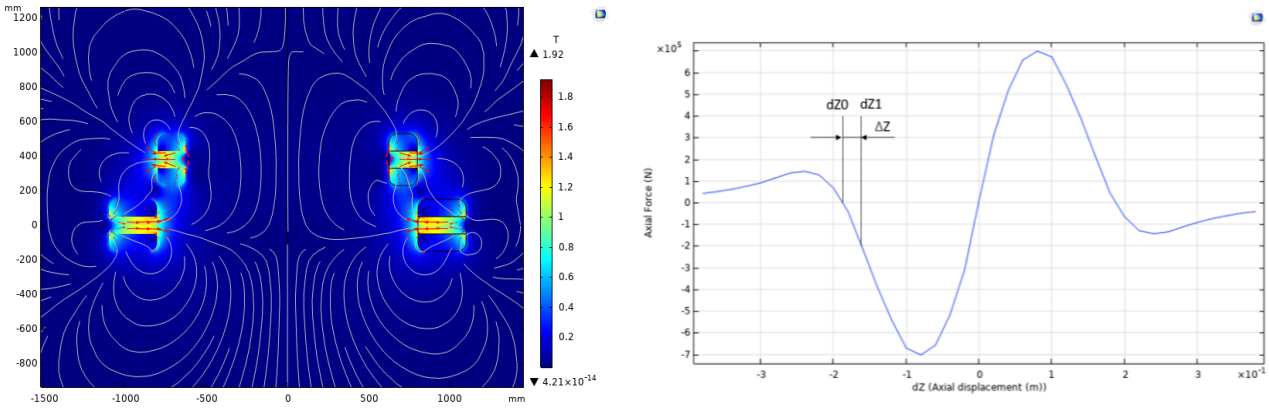

(a) (b)

Fig. 10. Plot of the axial PMB h_0 h_1 0.1 m, c 4mm, (a) magnetic flux density (b) axial force-displacement range *dZ* -0.38 to 0.38 m

Figure 11 is a plot of the axial force versus displacement generated in the axial PMB simulation with a magnetic thickness of 0.1 m which the width is varied for the magnetic gap "c" (4mm; 5mm; and 6mm) and for the distance set at *dZ* –190mm to -140mm. The rotor-stator distance that produces 0N (*LZ0*) magnetic axial force is 187mm. The measurement of *ΔZ* starts from the displacement point of the rotor-stator at an axial force of 0N (*dZ0*) to the location (*dZ1)* wherein F_Z 199.5 kN is produced. The thrust force on the HAWT main shaft, which is 199.5 kN, can be supported by axial PMB at *c* 4mm with displacement *ΔZ* 26mm, *c* 5mm with *ΔZ* 27mm, and *c* 6mm, the distance *ΔZ* is 28mm. Based on the simulation results, the minimum displacement against the thrust force is found at c 4mm. Furthermore, this configuration can support the axial load on the HAWT main shaft with a *ΔZ* value of 2.6mm.

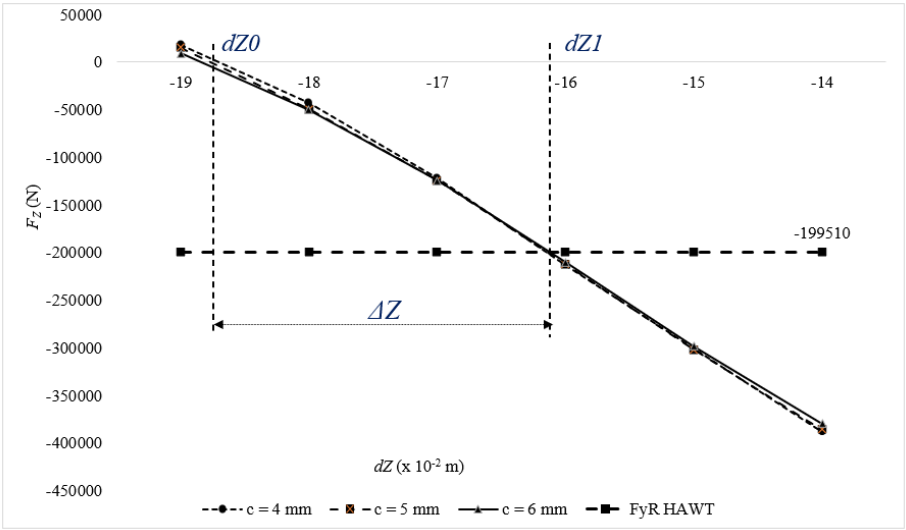

Fig. 11. The plot of the axial force-displacement of axial PMB, with h 0.1 m

3.5 Axial Force Modeling Of 0.15 M Magnet Thickness of the PMB

The axial PMB design uses the parameters provided in Table 1 have values of h0-h1 indicate a magnet thickness of 0.15 m. The difference in this configuration magnetic gap *c* values of 4mm, 5mm, and 6mm. Figure 12(a) shows the maximum magnetic flux density of 1.45T at 0.15 m thickness variation and 4mm gap, which is centered in the magnet's center on both the rotor and stator. Figure 12(b) shows the axial force-displacement which *dZ* – 0.38 m to 0.38 m.

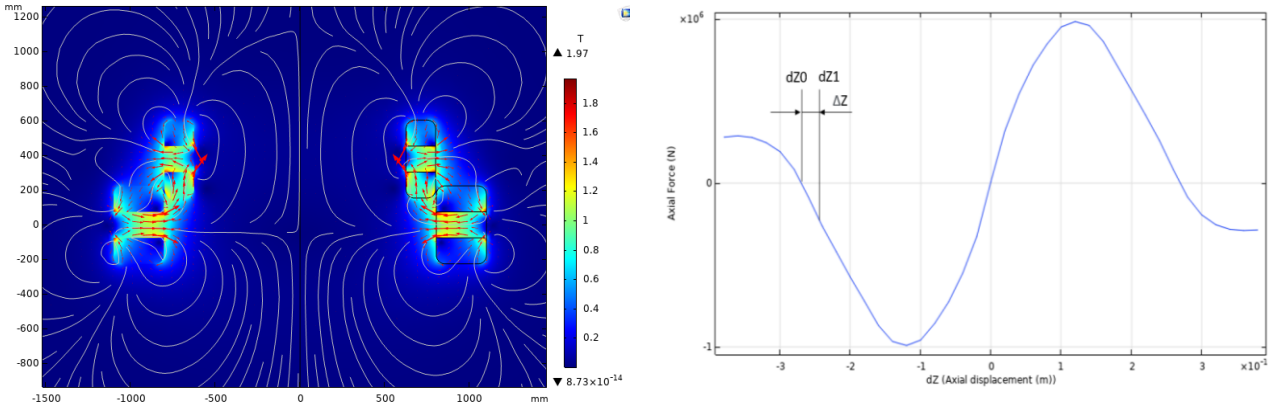

(a) (b)

Fig. 12. Plot of the axial PMB h_0 h_1 0.15 m, c 4mm, (a) magnetic flux density (b) axial force-displacement range *dZ* -0.38 to 0.38 m

Figure 13 shows a plot of the axial force against displacement created in the axial PMB simulation with a magnetic thickness of 0.15 m and a magnetic gap "*c*" (4mm; 5mm; 6mm) and a distance set at *dZ* – 270mm to -220mm. The rotor-stator distance required to generate (*LZ0*) 0 N magnetic axial force is 270mm.The thrust force of 199.5 kN on the HAWT main shaft may be sustained by axial PMB at c 4mm with displacement *ΔZ* 22mm, c 5mm with displacement *ΔZ* 22mm, and *c* 6mm with distance *ΔZ* 23mm. According to the results, the minimum displacement sustain the thrust force is discovered at *c* 4mm. Furthermore, with a *ΔZ* value of 22mm, this arrangement can sustain the axial load on the HAWT main shaft. The simulation results of the axial magnetic force at 0.15m thickness of the magnet is similar to 0.1m thickness configuration, wherein the air gap (*c*) the smaller the displacement smaller too.

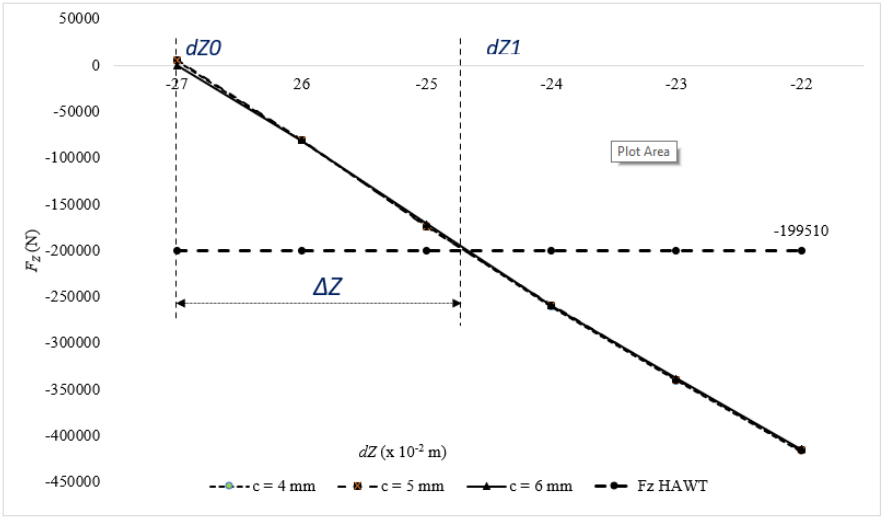

Fig. 13. Plot of the axial force -displacement of axial PMB, with h 0.15 m

3.6 Axial Force Modeling Of 0.2 M Magnet Thickness of the PMB

The axial PMB design proposes the specifications shown in Table 1, with h_0-h_1 indicating a magnet thickness of 0.2m. The magnetic gap c values of 4mm, 5mm, and 6mm differ in this arrangement. Figure 14(a) depicts the maximum magnetic flux density of 1.45T in the central magnetic region of the rotor and stator, for 0.2 m thickness variation and 4mm gap of the axial PMB Design. Figure 14(b) depicts the axial force-displacement relationship with *dZ* – 0.38 m to 0.38 m.

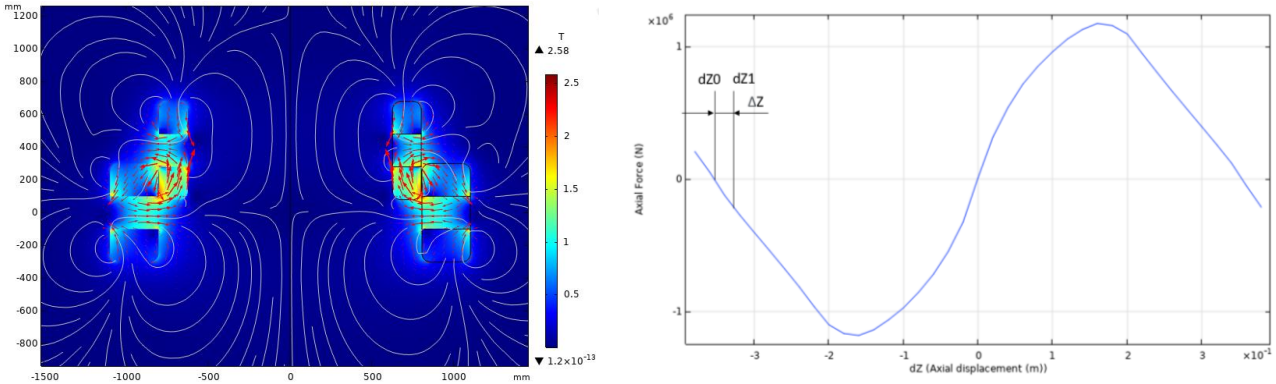

(a) (b)

Fig. 14. Plot of the axial PMB h_0 h_1 0.2 m, c 4 mm, (a) magnetic flux density (b) axial force-displacement range *dZ* -0.38 to 0.38 m

Figure 15 displays the plot of axial force versus displacement of the axial PMB simulation with a magnetic thickness of 0.2 m, a magnetic gap "*c*" (4mm; 5mm; 6mm), and a distance set *dZ* –360mm to -310mm. The distance between the rotor and the stator generates 0N magnetic axial force (*LZ0*) is 354 mm. The HAWT thrust force of 199.5 kN was sustained by axial PMB at c 4mm with displacement *ΔZ* 25mm, while at *c* 5 and 6mm, the displacement *ΔZ* was 26mm. The simulation results show that the thicker the PMB axial magnet, the greater the axial magnetic force.

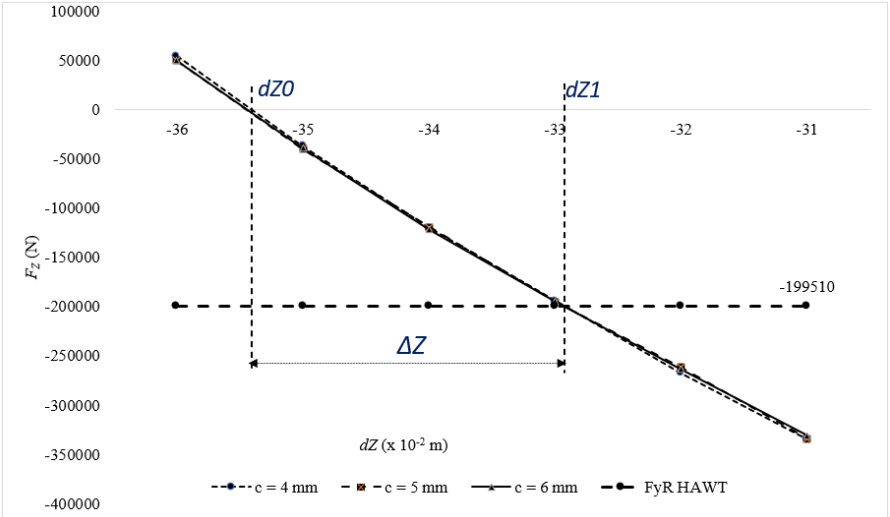

Fig. 15. Plot of the axial force -displacement of axial PMB, with h 0.2 m

The Magnetic axial force (F_z) from axial displacement (*dZ*) in the PMB axial design varied with the magnetic gap and magnetic thickness simulated using the finite element method. The magnetic thrust force must meet 199.5kN and the lowest displacement (*ΔZ*) in each configuration are limitations into consideration in selecting the PMB axial for the main shaft of the HAWT. Therefore,

the axial PMB with magnet thickness, h_0-h_1 of 0.15m, air gap of 4mm produces F_z value 199.5kN, with a minimum ΔZ value 22mm, which is the optimal configuration to obtain the lowest displacement as the HAWT axial bearing. Figure 15 depicts the smallest ΔZ displacement (22mm) in h1.5c4 and h1.5c5 variants, which are PMB axial designs with a thickness of 0.15m and a magnetic gap between the rotor and stator of 4 mm and 5 mm, respectively. Although ΔZ 22mm is the smallest, the flexibility range is still too wide to be utilized as a single substitute for HAWT's mechanical thrust bearing.

Figure 16 depicts the *LZ0* distance of 187mm on the Axial PMB 0.1m magnet thickness for the three magnetic gap changes (4,5,6mm), 270mm distance at 0.15m thickness, and 354mm distance at 0.2m thickness. The 0.1m magnet thickness has the lowest *LZ0* value. This demonstrates that the greater the thickness of the PMB axial magnet design, the greater the displacement that provides zero axial magnetic force, but is unaffected by changes in the magnetic gap (c). The rise in displacement value is proportional to the axial magnetic force produced, which increases with the size of the magnet's thickness (see Figure 17). However, there is small decrease produce in the axial magnetic force wherein the size of the magnetic gap (c) gets large. This result is similar to studies in that a smaller magnetic gap width will produce a higher magnetic force [7,35]. The effect of axial magnetic force fluctuation from magnetic gap variation is insignificant, with a difference of 3.16 % for axial PMB with a thickness of 0.1m, a difference of 2 % for a magnet thickness of 0.15m, and a difference of 1.69% for a magnet thickness of 0.2m.

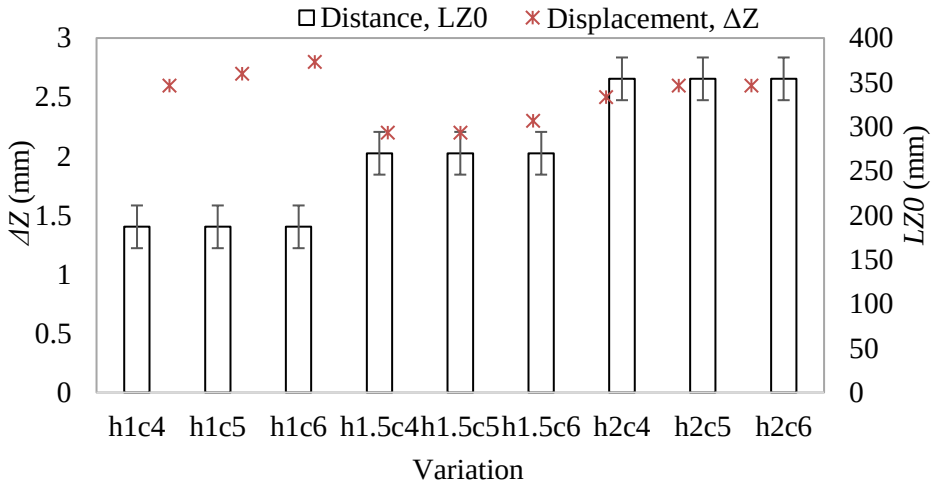

Fig. 16. Displacement *ΔZ* and distance *LZ0* of the axial PMB variations

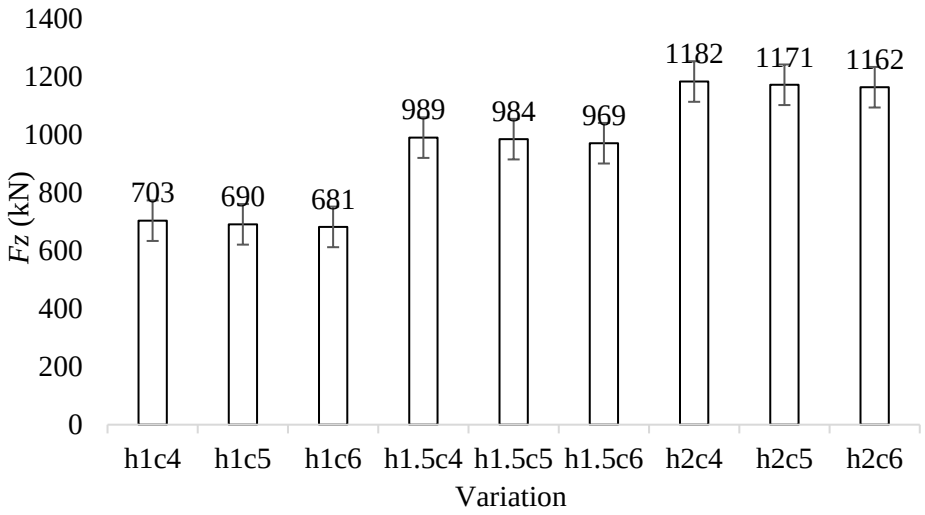

Fig. 17. The maximum of magnetic of the axial PMB variations

4. Conclusions

The permanent magnetic bearing as an axial bearing of the main shaft HAWT was designed to generate the magnetic force that resists the thrust forces from wind imposed on the rotor blades. The PMB model consists of rotor and stator magnets arranged in 3 layers that vary in thickness and width of the gap has been simulated base on the displacement of the rotor magnet against the stator. The PMB model with a thickness of 0.15m and a gap of 4mm has the shortest displacement, *ΔZ* (22mm) that produces a minimum axial magnetic force of 199.5 kN compared to other variations. However, this displacement has a considerable distance, so it is not feasible to use it as a single replacement for HAWT's axial bearing unless combined with the HAWT shaft main bearing close to the rotor. It is also feasible to decrease axial displacement by increasing the number of PMB axial models in one main axis of the HAWT. Analysis shows that the greater the magnet thickness of the PMB, the greater the magnetic axial force and the displacement that provides zero axial magnetic force. Furthermore, increasing the size of the rotor magnet gap towards the stator decreases the magnetic force even though small. The insignificant decrease in the value of the axial force is due to the variation of small gap magnet width. The highest decrease was found of the PMB model with a 0.1m thick magnet, where the magnetic force generated at a 4mm magnet gap compared to a 6mm magnetic gap decreased by 3.16%.

References

[1] Encalada-Dávila, Ángel, Bryan Puruncajas, Christian Tutivén, and Yolanda Vidal. "Wind Turbine Main Bearing Fault Prognosis Based Solely on SCADA Data." *Sensors* 21, no. 6 (2021): 2228. https://doi.org/10.3390/s21062228

[2] Tazi, Nacef, Eric Châtelet, and Youcef Bouzidi. "Wear analysis of wind turbine bearings." *International Journal of Renewable Energy Research (IJRER)* 7, no. 4 (2017): 2120-2129.

[3] Fekry, Mohamed, Abdelfatah M. Mohamed, Mohamed Fanni, and Shigeo Yoshida. "A comprehensive performance assessment of the integration of magnetic bearings with horizontal axis wind turbine." *Mathematics and Computers in Simulation* 156 (2019): 1-39.https://doi.org/10.1016/j.matcom.2018.06.011

[4] Zhang, Weiyu, and Huangqiu Zhu. "Radial magnetic bearings: An overview." *Results in physics* 7 (2017): 3756-3766. https://doi.org/10.1016/j.rinp.2017.08.043

[5] Jin, Chaowu, Yuanping Xu, Jin Zhou, and Changli Cheng. "Active Magnetic Bearings Stiffness and Damping Identification from Frequency Characteristics of Control System." *Shock and Vibration* 2016 (2016): 1-8. https://doi.org/10.1155/2016/1067506

[6] Alami, Abdul Hai. "Introduction to mechanical energy storage." *Reference Modeule in Earth Systems and Environmental Sciences.* Elsevier. 2021 https://doi.org/10.1016/B978-0-12-819723-3.00080-9

[7] Micha, Premkumar T., Thangaraj Mohan, and Seralathan Sivamani. "Design and analysis of a permanent magnetic bearing for vertical axis small wind turbine." *Energy Procedia* 117 (2017): 291-298. https://doi.org/10.1016/j.egypro.2017.05.134

[8] Kriswanto, and Jamari. "Radial forces analysis and rotational speed test of radial permanent magnetic bearing for horizontal axis wind turbine applications." In *AIP Conference Proceedings*, vol. 1725, no. 1, p. 020034. AIP Publishing LLC, 2016. https://doi.org/10.1063/1.4945488

[9] Daniel, Dan V., Nicolae Tănase, E. S. Apostol, Ionel Chiriţă, and Cristinel Ilie. "An overview regarding the analytical vs. numerical computation for a PMB used for FESS." In *2017 10th International Symposium on Advanced Topics in Electrical Engineering (ATEE)*, pp. 458-462. IEEE, 2017. https://doi.org/10.1109/ATEE.2017.7905044

[10] Teng, Wei, Xian Ding, Xiaolong Zhang, Yibing Liu, and Zhiyong Ma. "Multi-fault detection and failure analysis of wind turbine gearbox using complex wavelet transform." *Renewable Energy* 93 (2016): 591-598. https://doi.org/10.1016/j.renene.2016.03.025

[11] Bekinal, Siddappa Iranna, and Mrityunjay Doddamani. "Friction-free permanent magnet bearings for rotating shafts: A comprehensive review." *Progress In Electromagnetics Research C* 104 (2020): 171-186. https://doi.org/10.2528/PIERC20060402

[12] Parambil, Lijesh K. "Design methodology for monolithic layer radial passive magnetic bearing." *Proceedings of the Institution of Mechanical Engineers, Part J: Journal of Engineering Tribology* , (2019): 1-9. https://doi.org/10.1177/1350650118806372

[13] Zhang, Li, Huachun Wu, Peng Li, Yefa Hu, and Chunsheng Song. "Design, Analysis, and Experiment of Multiring Permanent Magnet Bearings by Means of Equally Distributed Sequences Based Monte Carlo Method." *Mathematical Problems in Engineering* 2019 (2019): 1-17. https://doi.org/10.1155/2019/4265698

[14] Wang, Ruiming, Tian Han, Wenrui Wang, Yang Xue, and Deyi Fu. "Fracture analysis and improvement of the main shaft of wind turbine based on finite element method." *Advances in Mechanical Engineering* 10, no. 4 (2018): 1–9. https://doi.org/10.1177/1687814018769003

[15] Anonymous. 2021. Ovako 34CrNiMo6 SB9205 Steel. http://www.matweb.com/search/DataSheet.aspx?MatGUID=e3376bb4f6ab4d9ba23f4b7aa7f1882a&ckck=1

[16] Ni, Qing, Ke Feng, Kesheng Wang, Binyuan Yang, and Yu Wang. "A case study of sample entropy analysis to the fault detection of bearing in wind turbine." *Case studies in engineering failure analysis* 9 (2017): 99-111. https://doi.org/10.1016/j.csefa.2017.10.002

[17] Ge, Yanming, and Kehong Wang. "Influence of Microalloying Element on the Microstructure and Mechanical Properties of 34CrNiMo6 Steel for Wind Turbine Main Shaft." *Advances in Materials Science and Engineering* 2018 (2018): 1-6. https://doi.org/10.1155/2018/2672385

[18] Chunping, Huang, Lin Xin, Liu Fencheng, Cao Jun, Liu Fenggang, and Huang Weidong. "Effects of cooling condition on microstructure and mechanical properties in laser rapid forming of 34CrNiMo6 thin-wall component." *The International Journal of Advanced Manufacturing Technology* 82, no. 5-8 (2016): 1269-1279. https://doi.org/10.1007/s00170-015-7453-z

[19] Branco, R., J. D. Costa, F. Berto, A. Kotousov, and F. V. Antunes. "Fatigue crack initiation behaviour of notched 34CrNiMo6 steel bars under proportional bending-torsion loading." *International Journal of Fatigue* 130 (2020): 105268. https://doi.org/10.1016/j.ijfatigue.2019.105268

[20] Aryadi, W., A. Roziqin, and J. Jamari. "Static Structural Analysis of the Sports Utility Vehicles Patriot Chassis." In *IOP Conference Series: Earth and Environmental Science*, vol. 700, no. 1, p. 012006. IOP Publishing, 2021. https://doi.org/10.1088/1755-1315/700/1/012006

[21] Roziqin, Ahmad, and W. Aryadi. "Finite element analysis of village car pickup ladder frame chassis-a case study." In *IOP Conference Series: Earth and Environmental Science*, vol. 700, no. 1, p. 012008. IOP Publishing, 2021. https://doi.org/10.1088/1755-1315/700/1/012008

[22] Roziqin, A., F. Hasyim, D. D. Saputro, and B. Wijayanto. "Static Structural Analysis and Determination of Low-Cost Component Sizes of The Paper Pulper Machines." In *IOP Conference Series: Earth and Environmental Science*, vol. 700, no. 1, p. 012004. IOP Publishing, 2021. https://doi.org/10.1088/1755-1315/700/1/012004

[23] Azizan, Azisyahirah, Haris Ahmad Israr, and Mohd Nasir Tamin. "Effect of Fiber Misalignment on Tensile Response of Unidirectional CFRP Composite Lamina." *Journal of Advanced Research in Applied Sciences and Engineering Technology* 11, no. 1 (2018): 23-30.

[24] Ibrahim, Mohamed Ibrahim J., and Mohd Zuhri Mohamed Yusoff. "Optimization of interlocking structures made of flax fibre composites to improve its energy absorption capability." *Journal of Advanced Research in Applied Sciences and Engineering Technology* 10, no. 1 (2018): 1-17.

[25] Veritas, Norske. *Guidelines for design of wind turbines*. Det Norske Veritas: Wind Energy Department, Risø National Laboratory, 2002.

[26] Nasri, Wiem, Ridha Djebali, Marjan Goodarzi, Mohamed Ammar Abbassi, and Said Abboudi. "Apple convective

drying-Part I: Finite elements parametric study for appraising the operating conditions effects." *CFD Letters* 11, no. 3 (2019): 28-41.

[27] Sardjono, P., F. Gulo, and D. Setiabudidaya. "Crystal structure and magnetic properties of Nd2Fe14B powder prepared by using high energy milling from elements metal Nd, Fe, B powders." In *Journal of Physics: Conference Series*, vol. 776, no. 1, p. 012013. IOP Publishing, 2016. https://doi.org/10.1088/1742-6596/776/1/012013

[28] Sardjono, P. "Physical and magnetic properties, microstructure of bonded magnet NdFeB prepared by using synthesis rubber." In *Journal of Physics: Conference Series*, vol. 776, no. 1, p. 012015. IOP Publishing, 2016. https://doi.org/10.1088/1742-6596/776/1/012015

[29] Wang, Xiaobai, Kai Zhu, Wei Li, Junjie Xu, Zeeshan Ali, and Yanglong Hou. "Nd2Fe14B hard magnetic powders: Chemical synthesis and mechanism of coercivity." *Journal of Magnetism and Magnetic Materials* 518 (2021): 167384. https://doi.org/10.1016/j.jmmm.2020.167384

[30] Jeong, Ji Hun, Hao Xuan Ma, Doyun Kim, Chang Woo Kim, In Ho Kim, Jae Woo Ahn, Dong Soo Kim, and Young Soo Kang. "Chemical synthesis of Nd 2 Fe 14 B hard phase magnetic nanoparticles with an enhanced coercivity value: effect of CaH 2 amount on the magnetic properties." *New Journal of Chemistry* 40, no. 12 (2016): 10181-10186. https://doi.org/10.1039/C6NJ02436J

[31] Krugel, Georg, Wolfgang Körner, Daniel F. Urban, Oliver Gutfleisch, and Christian Elsässer. "High-throughput screening of rare-earth-lean intermetallic 1-13-x compounds for good hard-magnetic properties." *Metals* 9, no. 10 (2019): 1096. https://doi.org/10.3390/met9101096

[32] Constantinides, Steve, and John De Leon. "Permanent Magnet Materials and Current Challenges Development of Magnet Materials." *Arnold Magnetic Technology, Denmark*. 2017.

[33] Schroeter, Hagen. "Permanent Magnets Materials and Magnet Systems." *IBS Magnet, Berlin.* 2007.

[34] Bekinal, Siddappa Iranna, Anil Rao Tumkur Ramakrishna, and Soumendu Jana. "Analysis of axially magnetized permanent magnet bearing characteristics." *Progress In Electromagnetics Research* 44 (2012): 327-343. https://doi.org/10.2528/PIERB12080910

[35] Zhang, Li, Huachun Wu, Peng Li, Yefa Hu, and Chunsheng Song. "Design, Analysis, and Experiment of Multiring Permanent Magnet Bearings by Means of Equally Distributed Sequences Based Monte Carlo Method." *Mathematical Problems in Engineering* 2019 (2019): 1-17. https://doi.org/10.1155/2019/4265698